INTERNATIONAL JOURNAL OF HYDROGEN ENERGY 48 (2023) 37625–37636

Available online at www.sciencedirect.com

ScienceDirect

journal homepage: www.elsevier.com/locate/he

Thermal design and heat transfer optimisation of a liquid organic hydrogen carrier batch reactor for hydrogen storage

Marco Gambini, Federica Guarnaccia, Michele Manno[*], *Michela Vellini*

University of Rome Tor Vergata, Via del Politecnico, 1, Rome, 00133, Italy

HIGHLIGHTS

- Thermal design of hydrogen storage systems based on LOHC batch reactors is analysed
- Design is optimised to ensure effective heat transfer and minimum power consumption
- Novel dimensionless parameter (Heat Transfer Ratio, HTR) is introduced
- A threshold HTR value is identified, above which only marginal gains are achieved
- The lumped-parameter model can be deployed in complex energy system dynamic models

ARTICLE INFO

Article history:
Received 13 January 2023
Received in revised form
26 July 2023
Accepted 16 August 2023
Available online 31 August 2023

Keywords:
LOHC
Hydrogen storage
Lumped-parameter model
Batch reactor
Design optimisation
Heat transfer

ABSTRACT

Liquid organic hydrogen carriers (LOHCs) are considered a promising hydrogen storage technology. Heat must be exchanged with an external medium, such as a heat transfer fluid, for the required chemical reactions to occur. Batch reactors are simple but useful solutions for small-scale storage applications, which can be modelled with a lumped-parameter approach, adequately reproducing their dynamic performance. For such reactors, power is consumed to circulate the external heat transfer fluid and stir the organic liquid inside the reactor, and heat transfer performance and power consumption are two key parameters in reactor optimisation. Therefore, with reference to the hydrogen release phase, this paper describes a procedure to optimise the reactor thermal design, based on a lumped-parameter model, in terms of heat transfer performance and minimum power consumption. Two batch reactors are analysed: a conventional jacketed reactor with agitation nozzles and a half-pipe coil reactor. Heat transfer performance is evaluated by introducing a newly defined dimensionless parameter, the Heat Transfer Ratio (HTR), whose value directly correlates to the heat rate required by the carrier's dehydrogenation reaction. The resulting model is a valid tool for adequately reproducing the hydrogen storage behaviour within dynamic models of complex and detailed energy systems.

* *Corresponding author.*
E-mail addresses: gambini@ing.uniroma2.it (M. Gambini), federica.guarnaccia@students.uniroma2.eu (F. Guarnaccia), michele.manno@uniroma2.it (M. Manno), vellini@ing.uniroma2.it (M. Vellini).

https://doi.org/10.1016/j.ijhydene.2023.08.200

1. Introduction

The development of reliable and competitive hydrogen technologies has been considered fundamental by nations all over the world, such as Japan [1], China [2], the UK [3], the USA [4], and EU members [5]. For the latter, a strong emphasis has been placed in recent months in response to the Ukrainian-Russian crisis [6]. Today, more than ever, reducing the influence of fossil fuels is mandatory to preserve our climate, our planet, and economic and social stability. Green hydrogen [7] can unlock the full potential of renewable energy sources, providing an effective way to store carbon-free electricity and decarbonise various energy sectors (such as, for example, the gas grid [8]) as a crucial tool in the wider context of sector coupling [9], in particular in so-called hard-to-abate sectors [10], such as heavy-duty transport [11].

Although sustainable hydrogen production and hydrogen-based technologies still require further research [12], hydrogen storage brings additional issues that need to be addressed, such as safety hazards and low energy density [13]. Traditionally, the two main pathways to store hydrogen are compressed [14] and liquid hydrogen [15], but both are lacklustre in terms of energy density, storage conditions, and efficiency. Bulk storage technologies using underground pipes or caverns are available and can be practical [16] and safe [17], but cannot be applied widely due to geographical limitations [18]. Consequently, alternative routes have been explored, such as Liquid Organic Hydrogen Carriers (LOHCs): in these molecules, double carbon-carbon bonds are reversibly broken to store hydrogen through exothermic reactions (hydrogenation). On the contrary, to release hydrogen, endothermic reactions must occur (dehydrogenation) as the double bonds are re-established [19]. LOHCs have already been scrutinised to assess their technical and economical performance as hydrogen storage systems: it has been found that distributing hydrogen from a hydrogen production plant to a terminal refuelling station with LOHCs is cheaper than compressed, liquefied or pipeline hydrogen for long-distance, large-volume (higher than 20000 kg/d) hydrogen demands [20], while they may achieve the lowest Levelised Cost of Hydrogen (LCOH) compared to compressed or liquefied hydrogen if the entire supply chain for green hydrogen production, storage, transportation and distribution is considered [21]. LOHCs are in particular very competitive compared to more established technologies for long-term, large-scale hydrogen storage [22]. However, relative to other hydrogen carriers, LOHCs require a significant heat demand at relatively high temperatures, and heat integration within each specific application plays an essential role to ensure that hydrogen is stored and distributed efficiently [18].

LOHCs were first proposed in the 1980s [23], although they have gained popularity only in the last few years [24]. Currently, Di-Benzyl-Toluene (DBT) [25] and N-Ethyl-Carbazole (NEC) [26] are the most studied carriers, although a multitude of other fluids have been assessed [27], also by means of a systematic evaluation of their physico-chemical properties [28]. Research is still ongoing not only for a carrier, but also for better catalysts [29], which are arguably mainly important during dehydrogenation [30] as higher temperatures are needed, and slow kinetics can prevent deep discharges [31,32], while the end-user requirements must be respected.

Although research on the chemistry of the process is still actively pursued, different case studies have been analysed to evaluate the performance of complex systems based on hydrogen turbines [33], or fuel cells [34]. Both papers focus mainly on the end-user application, but little information is reported about the actual behaviour of the carrier, allegedly modelled in 1D. Furthermore, the design proposed by Dennis et al. is characterised by an excessively cumbersome reactor [33]. On the contrary, Yang et al. focus on LOHC using a 2D model, although the influence of pressure on the reaction rate is omitted [35].

Although with different geometries, all the reactors mentioned above show a significant evolution of the Degree of Hydrogenation (DoH) in the axial direction with only moderate variation in the radial direction; consequently, they can be modelled as Plug Flow Reactors (PFRs). This design is in line with the traditional tubular and shell-and-tube heat exchangers and is suitable for relatively high flow rates of discharged hydrogen. However, simpler reactors, modelled as batch reactors, can provide effective storage solutions for small-scale hydrogen-based energy systems and are going to be required in a fully-fledged hydrogen economy.

Therefore, the aim of this paper is to present a procedure to optimise the thermal design of LOHC-based batch reactors, ensuring the required heat transfer performance and the lowest power requirement. The former is assessed through a novel dimensionless parameter, the Heat Transfer Ratio (HTR), while the latter is evaluated as the combination of pumping and stirring consumption. Hence, this paper does not deal directly with the chemical and kinetic characteristics of the reactor, which are assumed to be known for the LOHC and catalyst by means of a characterisation resulting in a set of parameters that can then be implemented in a model developed by the authors [36]. Instead, the focus here is on the thermal design of the reactor, and in particular on how to achieve the most efficient heat transfer process between the LOHC and the Heat Transfer Fluid (HTF), taking into account the power consumption from the stirring of LOHC inside the reactor and the HTF circulation.

The resulting lumped-parameter model is particularly useful, notwithstanding some unavoidable loss of detail, because it adequately reproduces the overall dynamics, thus making it possible to build dynamic models of complex energy systems, of which LOHC-based hydrogen storage systems only represent a component. So, these findings will be the starting point for more in-depth characterisations, including end-user requirements and control strategies in batch reactors, and thermal design considerations for continuous reactors.

2. Methods

2.1. *Reactor design*

The dehydrogenation reaction is endothermic and, therefore, heat must be supplied to the reactor to sustain the hydrogen

release from the carrier. In this paper, two alternative designs of a batch reactor were evaluated: jacketed and coiled reactors (Fig. 1), which differ in the way heat is provided to the system. The heat transfer correlations and the expected range of variability for each parameter were taken from Garvin, with reference to the conventional jacket with agitation nozzles and half-pipe coil designs [37].

As stated in the introduction, the optimisation process was conducted considering both the thermal performance of the reactor and the power consumption for the HTF circulation and the LOHC stirring. The power requirements for the agitation nozzles were deemed negligible.

The global optimum was found through Matlab's Global Optimisation Tool.

The sizing procedure, given the volume required to host the LOHC, for a given aspect ratio AR usually in the range of 1–4, starts with the evaluation of both the height H and the inner diameter D_i of the batch reactor (Fig. 1):

$$AR = H/D_i \tag{1}$$

$$V = \frac{\pi}{4}\frac{H^3}{AR^2}. \tag{2}$$

It should be noted that H is here defined in terms of the filling level, but the actual height of the reactor is likely to be somewhat higher to allow easier gas-liquid separation. Regardless, this upper empty space is almost unrelated to heat transfer performance and was then neglected in this analysis.

Having defined the wall thickness t_w (usually about 7 mm), the batch outer diameter is then easily derived:

$$D_e = D_i + 2t_w. \tag{3}$$

In the case of jacketed reactors, an additional diameter must be defined, that is, the outer diameter of the jacket D_j, which is evaluated as follows:

$$D_j = D_e + 2t_j \tag{4}$$

where t_j is the thickness of the jacket, which is usually in the 20–50 mm range. The heat exchange area A_{HX} is thus given by:

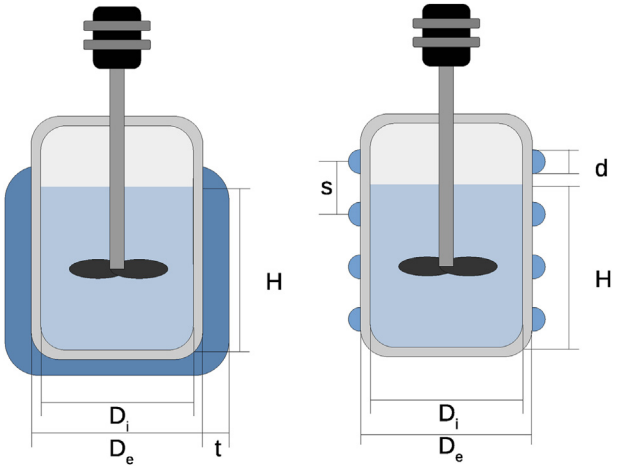

Fig. 1 – Batch reactor designs; going from left to right: jacketed batch reactor and coiled batch reactor.

$$A_{HX} = \pi D_e H \tag{5}$$

while the cross section A_f available to the HTF flow is obtained as:

$$A_f = H(D_j - D_e)/2. \tag{6}$$

For coiled-pipe reactors, instead, a tube diameter d must be chosen. Then, for a given pitch s representing the spacing between tubes, both the number of pipes N_p and the heat exchange surface A_{HX} are derived as follows:

$$N_p = \lfloor (H+s)/(d+s) \rfloor \tag{7}$$

$$A_{HX} = \pi D_e \left[(H - N_p d)\epsilon_f + N_p d \right]. \tag{8}$$

The pitch is usually in the range 35–50 mm. Eq. (8) highlights that well-designed reactor coils act as fins and even the residual wall surface participates in heat transfer exchange with efficiency ϵ_f. In this type of reactor, pipes do not have a circular section and are characterised by an angular opening (β). This value was set in this work as $\beta = 180°$; another common value is 270°. Most pipes have a diameter in the range 5.08–10.16 cm (2–4 in). The cross section available to the heat transfer fluid is:

$$A_f = \beta N_p \pi d^2/4. \tag{9}$$

Once the HTF velocity v_f is set, usually in the range 0.50–1.50 m/s, the mass flow rate is given, for both types of reactor, by:

$$\dot{m}_f = \rho_f A_f v_f \tag{10}$$

where ρ_f is the HTF density.

According to the lumped-parameter model implemented in this study, a homogeneous temperature T is assumed for the reactor, so the heat transfer process occurring between the HTF, which flows either in the jacket or in the coiled pipes, and the LOHC inside the reactor can be modelled as a single-stream heat exchanger [[38], p. 126]. Therefore, the effectiveness of heat transfer ϵ can be evaluated with the following simple expression as a function of the Number of Transfer Units NTU, which depends on the overall heat transfer coefficient U:

$$NTU = A_{HX}U/(\dot{m}_f c_f) \tag{11}$$

$$\epsilon = 1 - \exp(-NTU). \tag{12}$$

The overall heat transfer coefficient U in Eq. (11) accounts for the convective heat transfer from the HTF to the batch reactor (h_f), conduction through the wall (λ_m) and, lastly, inner convection through the carrier (h_l).

$$U = \left(\frac{1}{h_f} + \frac{D_e \ln(D_e/D_i)}{2\lambda_m} + \frac{D_e}{D_i}\frac{1}{h_l} \right)^{-1} \tag{13}$$

Values of λ_m have been obtained assuming a stainless steel 316L reactor; heat conductivity at working temperature is evaluated using data available in the literature [39].

The heat transfer coefficients in Eq. (13) are evaluated with empirical formulae for HTF [37] and LOHC [40] that allow the evaluation of the Nusselt number $Nu = hd_{hyd}/\lambda$ based on the chosen reactor type (coiled or jacketed).

In coiled reactors, the HTF heat transfer coefficient is a function of the Reynolds number (evaluated through the hydraulic diameter d_{hyd}), the Prandtl number, and the ratio between the hydraulic and curvature diameters:

$$\mathrm{Nu}_f = 0.0225\,\mathrm{Re}_f^{0.795}\mathrm{Pr}_f^{0.495}\exp\left[-0.0225(\log\mathrm{Pr}_f)^2\right]\left\{1 + 0.059\left[\mathrm{Re}_f(d_{hyd}/d_c)^2\right]^{0.34}\right\} \quad (14)$$

$$\alpha_c = \arctan\left(\frac{2H}{\pi D_i}\right) \quad (15)$$

$$d_c = D_i/\cos(\alpha_c). \quad (16)$$

In the case of jacketed reactors, the convective heat transfer coefficient can be estimated from empirical formulae as a function of the Reynolds number, the Prandtl number, and an entrance correction (Ge_f), as follows:

$$\mathrm{Nu}_f = 0.0192\,\mathrm{Re}_f^{0.795}\mathrm{Pr}_f^{0.495}\exp\left[-0.0225(\log\mathrm{Pr}_f)^2\right]\left\{1 + 0.059[\mathrm{Re}_f(d_{hyd}/D_i)^2]^{0.34}\right\}Ge_f \quad (17)$$

$$Ge_f = \begin{cases} 1, & \mathrm{Re}_f\left(d_{hyd}/d_c\right)^2 \le 4.72 \\ 1 + 5.71\dfrac{d_{hyd}}{\pi D_e}\left[1 - \exp\left(1 - 0.07(\pi D_e)/d_{hyd}\right)\right], & \mathrm{Re}_f\left(d_{hyd}/d_c\right)^2 > 4.72. \end{cases} \quad (18)$$

On the contrary, heat transfer through the carrier adheres to the same mechanism in both reactors. Assuming natural convection to be negligible, h_l is evaluated from Eq. (19) [40]. Since motion is related to angular velocity, the rotational Reynolds number Re_ω, which depends on the impeller rotational speed n, is introduced in Eq. (20).

$$\mathrm{Nu}_l = 0.11\left[(\mathrm{Re}_\omega^2/2 + \mathrm{Gr})\mathrm{Pr}_l\right]^{0.35} \quad (19)$$

$$\mathrm{Re}_\omega = D_i^2 n\rho_l/(2\mu_l). \quad (20)$$

Due to the uniform heat exchange over the height of the reactor in the batch configuration, natural convection does not play any significant role in heat transfer. As such, the Grashof number (Gr) is set to zero. The rotational speed is evaluated through Eq. (31) as explained in the following paragraphs.

The pumping power, required to circulate a HTF mass flow rate $\dot{m}_f$ through the jacket or the external pipes, is evaluated from Eq. (21), having defined the concentrated (Δp_C) and the distributed (Δp_D) pressure losses in Eqs. (22) and (23), The fanning friction factor is calculated either through Eq. (24) for jacketed reactors or Eq. (25) for coiled reactors:

$$P_{circ} = \dot{m}_f(\Delta p_C + \Delta p_D)/\rho_f \quad (21)$$

$$\Delta p_C = 4K_{elbow}\rho_f v^2/2 \quad (22)$$

$$\Delta p_D = f\frac{\pi(D_e + d)}{d_{hyd}}\rho_f\frac{v^2}{2} \quad (23)$$

$$f = \left(1.8\log_{10}\mathrm{Re}^* - 1.5\right)^{-2} \quad \text{(jacketed reactors)} \quad (24)$$

$$f = \begin{cases} 16/\mathrm{Re}, & 0 < \mathrm{Re} < 2100 \\ 0.0791/\mathrm{Re}^{0.25}, & 2100 \le \mathrm{Re} \le 1\times10^7 \\ 0.0014 + 0.125/\mathrm{Re}^{0.32}, & \mathrm{Re} > 1\times10^7 \end{cases} \quad \text{(coiled reactors)}. \quad (25)$$

The curvature effect is accounted for by the coefficient K_{elbow} in Eq. (22) as a tabulated value function of hydraulic and external diameter (d_{hyd},D_e) for a 90° bending using data taken from White [41]. Regarding the Gnielinski correlation, Eq. (24), the value of Re* must be evaluated as follows:

$$\mathrm{Re}^* = \frac{\left[1 - (D_e/D_j)^2\right] + \left[(1 + D_e/D_i)^2\right]\log D_e/D_i}{\left[1 - (D_e/D_j)^2\right]\log D_e/D_j}\,\mathrm{Re}. \quad (26)$$

It must also be noted that the hydraulic diameter defined for pressure loss evaluation is not the same as that required for heat transfer analysis, since the reference wet perimeter is different.

An impeller is required to mix the bulk liquid to promote homogeneity and improve the reaction operating conditions. Its power consumption scales with its diameter, rotational speed, LOHC density, and viscosity. This paper uses correlations available in the literature [42], assuming a Half Hold-up impeller:

$$d_{imp} = D_i/3. \quad (27)$$

Power consumption is evaluated from empirical equations based on three dimensionless numbers: the power number (N_p), the impeller-imposed Reynolds number Re_{imp} and the Froude number Fr, defined as follows:

$$N_p = P_{st}/\left(\rho_l n^3 d_{imp}^5\right) \quad (28)$$

$$\mathrm{Re}_{imp} = \rho_l n d_{imp}^2/\mu_l \quad (29)$$

$$\mathrm{Fr} = d_{imp}n^2/g. \quad (30)$$

Stirring has been shown to have a key influence on reaction rate [43]. Currently, no information is available on the advised correlation between rotational speed and reactor size. Since laboratory tests are carried out on small samples, it is reasonable to assume that the actual stirring conditions could be characterised by a low rotational speed (10.0–16.6 Hz is advised by Wan et al. [43]) to limit the tip velocity.

As such, the rotational speed was evaluated by imposing a supercritical regime, defined as the transition between non-aerated (subcritical) and aerated (supercritical) conditions:

$$n_{cr} = (S/K)^{\frac{7}{10}}(\mu_l/\rho_l)^{\frac{1}{21}} g^{\frac{10}{21}} d_{imp}^{-\frac{4}{7}} \tag{31}$$

where S and K are empirical parameters: for the Half Hold-up impeller, $K = 13.5$, $S = 9.5$. As seen from Eq. (31), it is safe to assume a reduced required rotational speed as the size of the system increases. The critical rotational speed n_{cr} is also a function of the liquid thermophysical properties (viscosity and density) and the type of impeller through the empirical coefficients S and K. Therefore, the power consumption is deduced from Eq. (28), with the power number evaluated as the minimum value resulting from Eqs. (32) and (33), valid for $500 < \mathrm{Re}_{imp} < 250000$:

$$N_p = K\,\mathrm{Re}_{imp}^{-0.3} \tag{32}$$

$$N_p = S\left(\mathrm{Re}_{imp}\mathrm{Fr}\right)^{-1/3}. \tag{33}$$

2.1.1. *Thermophysical properties*

Dowtherm™ Q was considered as the heat transfer fluid and its properties were evaluated using CoolProp libraries [44].

Instead, since no reliable and comprehensive database is currently available for the main thermophysical properties of NEC (namely density ρ_l, viscosity μ_l, specific heat capacity c_l, and thermal conductivity λ_l), a group-contribution method was implemented [45]. Dynamic viscosity, density, and specific heat capacity have been evaluated with the Joback method, while thermal conductivity values are based on Gharagheizi. Both modelling procedures provide a reasonable estimate for organic liquids, assuming a temperature-dependent behaviour; methodology and data are taken from Green and Perry [[45], Section 2].

The overall binary mixture made out of the fully loaded and unloaded carrier is then characterised by assuming a mass-weighted average for c_l in Eq. (34), the effective mass-to-volume ratio for ρ_l in Eq. (35), Gambill's method for μ_l in Eq. (36) [46], and Vredeveld's for λ_l in Eq. (37) [47]:

$$c_l = \sum_i x_{m,i} c_i \tag{34}$$

$$\rho_l = \left(\sum x_{m,i}/\rho_i\right)^{-1} \tag{35}$$

$$(\mu_l/\rho_l)^{-1/3} = \sum_i x_{m,i}(\mu_i/\rho_i)^{-1/3} \tag{36}$$

$$\lambda_l = \left(\sum_i x_{m,i}\lambda_i^{-2}\right)^{-1/2,} \tag{37}$$

with $x_{m,i}$ being the mass fraction of the component in the mixture and ν_i its kinematic viscosity.

2.2. *Kinetic and thermodynamic model*

Most LOHC-based literature features a plug-flow reactor coupled with one-dimensional modelling to account for axial gradients. However, in a batch reactor, gradients are expected to arise mainly over the radial direction.

Both hydrogenation and dehydrogenation rates depend on temperature; heat is transferred to or from the system as the reactions occur. As a result, heat and mass transfers are mutually dependent in LOHC systems, as in MHs [48].

When heat is exchanged with the system through convection and propagated inside the system through conduction, the accuracy of a lumped parameter approach is usually estimated with the Biot number $\mathrm{Bi} = hL/\lambda$. No experimental data are available for the conductivities of LOHCs at high temperatures; however, using the model provided by Berger Bioucas et al., the conductivity can be estimated as $\lambda \cong 0.09$ W/(mK) at approximately 480 K [49]. Even assuming low values of the convective heat transfer coefficient such as $h \cong 1$ kW/(m^{2}K), the Biot number is bounded to be much higher than one taking into account reasonable values of characteristic lengths (for example, the optimal inner diameter obtained in section 3.2 is approximately 10 cm, resulting in $\mathrm{Bi} \approx 10^3$).

Nevertheless, a lumped-parameter approach is effective because of the internal heat sink provided by the endothermic reaction, taking into account that the overall reaction heat depends on temperature. If more hydrogen is released (higher temperature), more heat is sunk, thus slowing down the heating action ensured by the external liquid. This balancing mechanism allows for 0D modelling of MHs [48].

The dehydrogenation reactions occurring within the reactor can be represented by a lumped parameter model resulting in the following equation [36], which gives the reaction rate as a function of a pre-exponential factor k_0 that depends on the reaction and catalyst used, of temperature through the Arrhenius law, and of pressure through an exponential term involving a pressure coefficient b. The reaction rate can be expressed as the time derivative of the Degree of Hydrogenation DoH, which is the ratio of the current hydrogen content $m_{H_2}(t)$ to the maximum possible hydrogen content for a given storage technology. For a reaction of order n it can be thus expressed as:

$$\frac{\mathrm{dDoH}}{\mathrm{dt}} = -k_0 \exp\left(-\frac{E_a}{RT}\right)\exp(-bp)\,\mathrm{DoH}^n. \tag{38}$$

Conversion from the degree of hydrogenation DoH and its time derivative to hydrogen mass and mass flow rate requires the introduction of the maximum gravimetric hydrogen density w and the LOHC overall mass m_l, resulting in the following expression for the hydrogen mass flow rate $\dot{m}_{H_2}$ released by the system:

$$\dot{m}_{H_2} = -w m_l \frac{\mathrm{dDoH}}{\mathrm{dt}} = w m_l k_0 \exp\left(-\frac{E_a}{RT}\right)\exp(-bp)\,\mathrm{DoH}^n. \tag{39}$$

The energy conservation equation must take into account the system's heat capacity C, the heat absorbed by the endothermic dehydrogenation reaction that depends on reaction enthalpy ΔH_r and rate of reaction, and the heat supplied by the heat transfer fluid:

$$C\dot{T} = -\dot{m}_{H_2}\left[\Delta H_r + (c_p - c_v)(T - T_0)\right] + \epsilon \dot{m}_f c_f (T_{f,i} - T) \tag{40}$$

where the heat transfer effectiveness is evaluated according to Eq. (12).

The reactor model is thus made up of Eqs. (38)–(40), representing an ODE system that can be solved with an explicit third-order Runge-Kutta scheme.

2.3. Heat Transfer Ratio

The Heat Transfer Ratio HTR, defined in Eq. (41) and rewritten as Eq. (42), was deduced from the reactor thermal balance to assess the heat transfer performance. The HTR represents the ratio of the heat rate transferred by the HTF, per unit temperature difference between the HTF and the reactor, to the maximum heat rate generated by the dehydrogenation reaction, divided by the design temperature T_{des} to obtain a dimensionless quantity:

$$\mathrm{HTR} = \frac{\dot{Q}_{ext.fluid}}{\dot{Q}_{reaction,max}} \cdot \frac{T_{des}}{T_{f,i} - T} \tag{41}$$

$$\mathrm{HTR} = \frac{\epsilon \dot{m}_f c_f}{\Delta H_r \dot{m}_{H_2,\max} / T_{des}}. \tag{42}$$

Therefore, the numerator is the product of heat transfer effectiveness ϵ and HTF flow heat capacity $\dot{m}_f c_f$, while on the denominator side, the maximum heat rate depends on the heat of reaction ΔH_r and the maximum hydrogen flow rate, which is obtained, based on Eq. (39), at the beginning of the dehydrogenation process thanks to the highest value of DoH, provided that the reactor is heated to the desired reaction temperature beforehand, so that $T(t = t_0) = T_{des}$:

$$\dot{m}_{H_2,\max} = \dot{m}_{H_2}(t = t_0) = w m_l k_0 \exp\left(-\frac{E_a}{R T_{des}}\right) \exp(-bp)\, \mathrm{DoH}_{max}^n. \tag{43}$$

By this definition, HTR can be used to assess the heat transfer performance not only for different reactor sizes, but also for different LOHCs with similar reaction kinetic characteristics (for example, the same reaction order).

Alternative definitions of HTR were also tried. For example, the definition $\mathrm{HTR} = \dot{m}_f c_f \varepsilon / (m_{H_2} \mathrm{HHV})$ leads to an apparently much more straightforward parameterisation. The effective heat capacity is divided by the energy content of the system, thus removing sizing effects, but the resulting value is not dimensionless. More importantly, since different LOHCs vary in both release trends and reaction heat, the kinetic performances achieved with similar HTR for different carriers may lead to significantly different results.

Despite the more complex definition and the need to collect data on the kinetic release parameters, Eq. (42) was considered to be overall more significant due to the greater amount of information returned and the potential to be applied to different LOHCs.

To improve the heat transfer performance, higher values of HTR can be achieved as:

- more heat is provided through a higher HTF flow heat capacity, better effectiveness of the exchanger, or both;
- the reaction temperature is set to a higher value;
- a reduced temperature drop takes place;
- less reaction heat is sunk.

Consequently, while the first two bullet points are likely detrimental in terms of the system's costs and overall efficiency, the remaining scenarios are actually desirable.

Finally, as discussed in Section 3, it should be noted that the HTR is introduced as a measure of the kinetic performances of a real LOHC system with respect to its corresponding constant-temperature equivalent system.

3. Results and discussion

3.1. Heat Transfer Ratio analysis

The heat transfer performance of the reactor was analysed through the HTR: in particular, the effect of an increase in HTR, leading to an improvement in the heat transfer between HTF and LOHC, was studied to identify a threshold HTR value, representing the best trade-off between thermal design and kinetic performance, above which the improvement kinetic response is not significant.

To this end, the impact of HTR on reactor performance was first assessed in a test case represented by a storage system with an available hydrogen content of $m_{H_2} = 282.1$ g, which corresponds to a net energy output of 5 kWh by a fuel cell with a 45% HHV-based efficiency; the required LOHC mass is $m_l = m_{H_2}/w = 4.855$ kg. The parameters required to model this test case are listed in Table 1. The batch reactor is subjected to a spontaneous constant-pressure discharge process, that is, the discharged hydrogen flow rate is not controlled ad results from the instantaneous operating conditions, namely temperature and DoH, according to Eq. (39). The duration of discharge is set at 180 min.

Fig. 2 shows the influence of the HTR on how dehydrogenation and reactor temperature proceed with time; the temperature trend is remarkably similar to data available in the literature [51], albeit for a PFR, providing an indirect validation for the model presented. The different discharged hydrogen content is clearly a result of different temperature trends. With higher HTR values, the temperature drop for a given system progressively decreases. Consequently, faster kinetics is ensured, and a higher mass of hydrogen is discharged by the 180 min mark, by which a 0.2 DoH threshold can be reached using either NEC [32] or DBT [34] as carriers (Fig. 2 shows the behaviour of a reactor based on NEC). As HTR increases, the gap between different temperature profiles is reduced, and the overall temperature does not stray far from the original design temperature T_{des}: the kinetic performance thus progressively tends to a constant-temperature trend, and only marginal improvements become possible with a further increase in HTR. Further raising the HTR above about 100 for this system, either through a higher HTF mass flow rate or more expensive design choices, would not lead to practical gains. In this way, a threshold value can be identified, which in this case is $\mathrm{HTR}_{thr} \approx 100$.

The HTR parameter can be used to compare different LOHCs. Fig. 3 shows the final DoH reached by reactors containing NEC or DBT in the 180 min constant-pressure discharge described above, compared to the value that could be obtained in a constant-pressure, constant-temperature discharge process (dashed lines). Looking at the performance

Table 1 – Input parameters for the HTR assessment (NEC reactor).

Parameter	Value	Parameter	Value
Available H_2 mass m_{H_2}	282.1 g	Gravimetric density w [32]	5.81%
Enthalpy of reaction ΔH_r [50]	50.6 kJ/mol	Reaction order n [36]	2
Pre-exponential factor k_0 [36]	2.61×10^{12} min^{-1}	Activation energy E_a [36]	121.0 kJ/mol
Pressure coefficient b [36]	1.397 bar^{-1}	Initial DoH	95%
Duration of discharge	180 min	Reactor AR	1.7
Initial temperature	473 K	Hydrogen pressure	1.0 bar
HTF inlet temperature $T_f^{T_{des}}$	473 K	HTF mass flow rate $\dot{m}_f$	0.718 kg/s

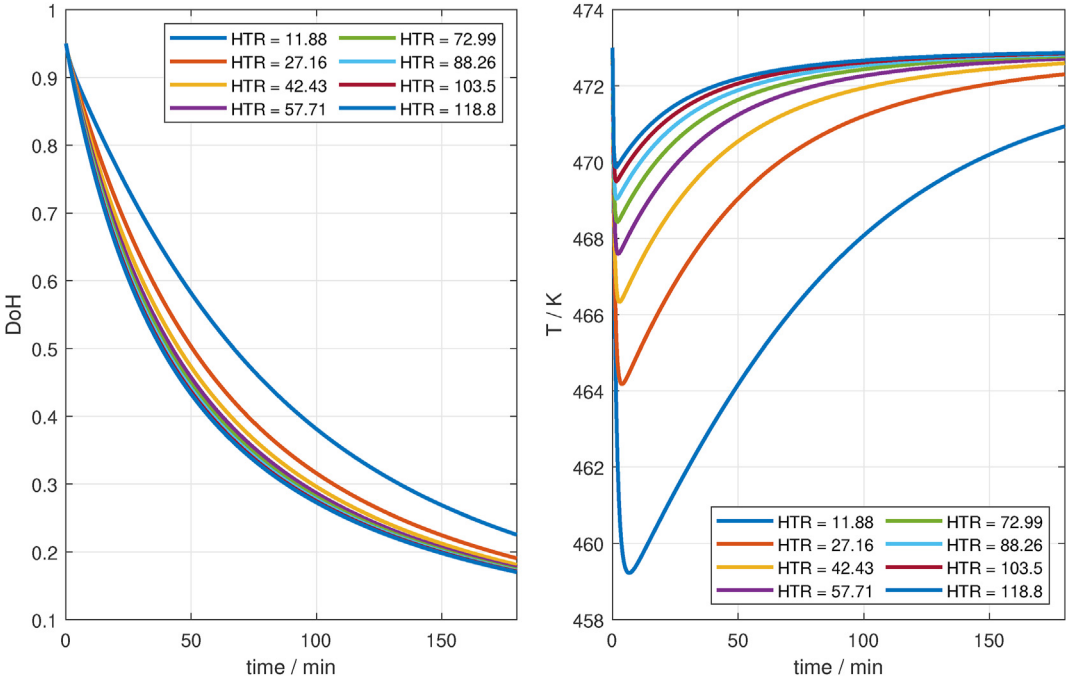

Fig. 2 – DoH and temperature evolution over time for different values of the HTR parameter.

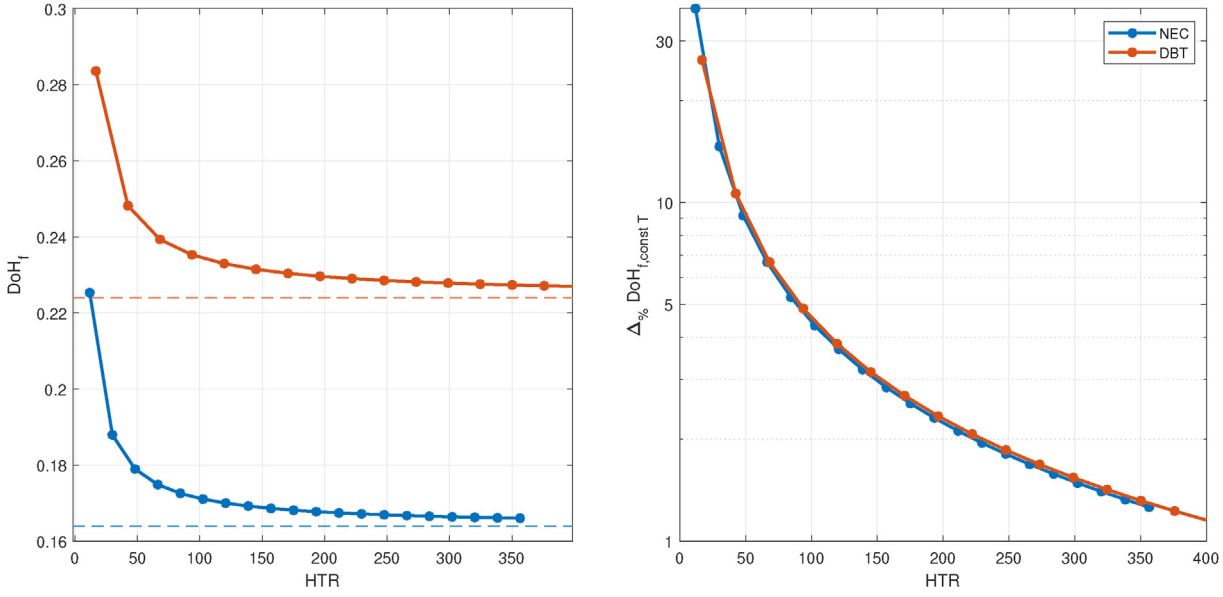

Fig. 3 – HTR influence over NEC and DBT systems. Dashed lines represent constant-temperature simulations. Left: DoH reached at t = 180 min for different values of HTR; right: deviation of the real reactor from the DoH reached in an ideal constant-temperature reactor.

of NEC and DBT, a threshold HTR value of about 90–100 is needed in both cases to achieve a final deviation lower than 5% with respect to the constant-temperature release profile. The temperature levels were chosen to ensure a final DoH($t = 180$ min) ≈ 0.20 at $p = 1.00$ bar, corresponding to 473 K*and*583 K respectively for NEC and DBT, given their different thermodynamic properties. In particular, Fig. 3 shows, on the left, how the higher HTR decreases the final degree of hydrogenation asymptotically with respect to the performance of the constant-temperature profile. As such, significant improvements are achieved only at low HTR values (≤ 100), above which the performance is already similar to those granted by a constant-temperature discharge. On the right, it shows the relative difference in final DoH between the tested reactor and the constant-temperature process: the remarkable similarity between the curves representing NEC and DBT shows that the HTR is useful in assessing heat transfer performance for different LOHCs, at least when the reaction order is similar (the reaction order for DBT has been shown to be very close to 2 [34]); preliminary results for other carriers hint at a possible correlation between the reaction order and the threshold value.

Consistent with the lumped-parameter approach and the definition of HTR, which is independent of size, both the scaling up and down of the sample leads to the same kinetic performance if the HTR parameter is kept constant. For any given size, the greater the HTR, the more limited the temperature drop will be. Consequently, higher temperature levels enhance the kinetic performance of the system. Since a relatively high heat demand is the main drawback of LOHC-based systems, it is crucial to strike the right balance between energy costs and release kinetics.

Only marginal kinetic improvements are achieved for higher values of the HTR, and, as such, a threshold value is defined to mark this saturation effect. Although the actual best choice for the HTR_{thr} value might differ to account for specific operating conditions and control strategies, a threshold value of $HTR_{thr} = 100$ was used in this article, allowing for a deviation from the DoH reached in an ideal constant-temperature reactor $\Delta_{\%}DoH_{i,const}T \leq 5\%$.

It must be reiterated that HTR is intended to be a tool for assessing how close the actual kinetic performance of the system is to that of an ideal, constant-temperature reactor. However, the amount of heat required is strictly correlated to the carrier itself and the reaction temperature: further and broader analyses are needed to optimise the efficiency of the whole system.

3.2. *Heat transfer optimisation*

As mentioned in section 2.1, the reactor design has been optimised in terms of heat transfer performance and mechanical power consumption, with reference to HTF circulation, Eq. (21), and LOHC stirring, Eq. (28). More precisely, the preceding section demonstrated that achieving a threshold HTR value guarantees the best trade-off between heat transfer performance and design requirements: therefore, the optimisation procedure relied on the overall power consumption as the objective function to be minimised:

$$\min P(\mathbf{x}) = \min\{P_{circ}(\mathbf{x}) + P_{st}(\mathbf{x})\} \tag{44}$$

with a non-linear constraint represented by the requirement that

$$HTR(\mathbf{x}) = HTR_{thr}(\mathbf{x}) = 100. \tag{45}$$

The decision variable is the array $\mathbf{x}$ containing the mutually-independent geometric properties of the reactor (aspect ratio AR, diameter D_i, and so on).

The optimisation results displayed in Table 2 show that the half-pipe coiled reactor is a better solution in terms of energy savings due to a power requirement that is almost halved. The gap between the two options is likely to be even greater, since the power supply to the agitation nozzles was neglected. These results indicate that in a LOHC system, the reactor can operate with little power and energy requirements. As a check of the consistency of the results, impeller power consumption was also evaluated with Nagata's correlations [52], obtaining a similar outcome.

Table 2 shows the same optimal AR value for the two layouts. This result is due to the greater contribution of the stirring power to the overall power consumption P, since it is mainly related to the diameter of the stirrer. A slightly lower P is required to operate the coiled reactor since better heat performances can be achieved: as such, a higher mass flow rate is required for the jacketed reactor. Furthermore, to achieve the target HTR, both the jacket width and the diameter of the pipes are set at the upper limit of their variability range. In contrast, the optimal pitch value could actually be replaced by an optimal range (as seen in Figs. 4 and 5) correlated with the same number of pipes.

Running local optimisation processes shows that similar results can be achieved with multiple parameter combinations. Consequently, if additional constraints on heat transfer performance or other aspects such as material usage and volume, or both, were introduced, different choices might be best suited. Therefore, those alternative designs would not significantly impact the energy demand of the system and the overall storage efficiency. Increasing the size of the system requires further analysis, since large-scale batch reactors may not be commercially available or sufficiently effective in terms

Table 2 – Results of the reactor optimisation process.

Parameter	Jacketed reactor	Half-pipe coiled reactor
	Value	Value
Height H/cm	39.22	39.22
Inner diameter D_i/cm	9.81	9.81
Outer diameter D_e/cm	11.21	11.21
Aspect ratio AR	4.00	4.00
HTF velocity v_f/(m/s)	2.05	2.40
HTF mass flow rate $\dot{m}_f$/(kg/s)	16.97	16.12
Power consumption P/W	2.3	0.9
Jacket width t/cm	5.0	–
Pipes diameter d/cm	–	10.16
Pipes pitch s/cm	–	4.93
Overall heat transf. coeff. U/(kW/(m^2 K))	6.21	6.38
HTR	100.0	100.0

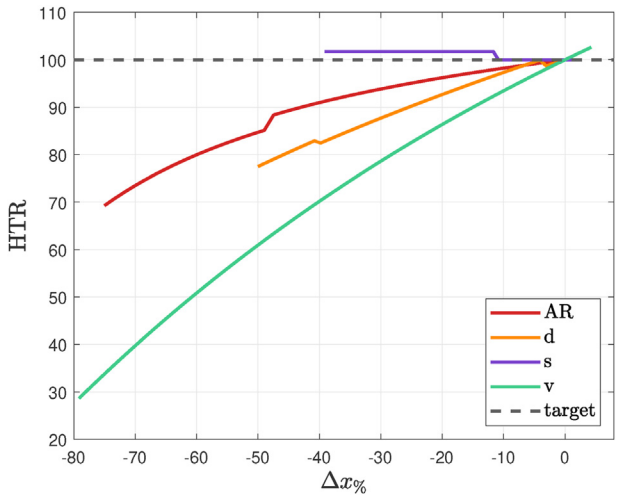

Fig. 4 – Influence of different parameters on heat transfer.

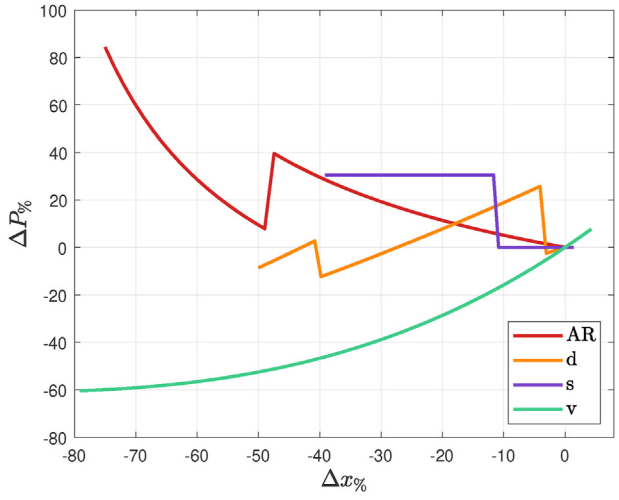

Fig. 5 – Influence of the different parameters on the power consumption with respect to its optimal value.

of overall efficiency. Therefore, additional requirements should also take into account parallel reactor configurations.

A sensitivity analysis was run to evaluate the influence of each parameter over the HTR and the power requirements, varying each parameter in its range and setting the others to their optimal value.

Fig. 4 shows the results obtained for HTR: for a set value of the other parameters, both AR and the diameter of the pipes have a great influence on the actual performance of the heat transfer process. On the contrary, due to the limited variability for the set size of the reactor, the pitch has a limited impact on the final outcome. On the other hand, the HTF velocity v_f is the most important parameter, with the HTR displaying an almost linear dependency. In fact, higher velocities lead to both a higher mass flow rate and better convection. Increasing the velocity, aspect ratio, or diameter of the pipes leads to better performance. On the other hand, increasing the pitch reduces HTR as long as a smaller number of pipes fits the batch height. The discontinuities that arise are a consequence of the number of pipes, Eq. (7), being an integer value resulting from a rounding operation.

Fig. 5 shows the impact of the same parameters on power consumption and reaffirms the importance of AR and d. The pitch has a more limited influence, while HTF velocity still has the most significant impact on the final result in the same way as explained in the previous paragraph. Combining this result with Fig. 2 leads to a key finding: increasing heat transfer to maintain a constant temperature is both pointless and highly detrimental in terms of power consumption, as the most reliable way to increase HTR is through the HTF velocity. As such, even for suboptimal geometric configurations, limited variability in the energy costs is expected.

4. Conclusions

Reactors are key elements in LOHC-based systems. This paper provides a streamlined design procedure to optimise two types of batch reactors using a lumped-parameter approach.

The lumped-parameter model is effective enough to guide the preliminary design stage, and the optimisation process leads to minimising the system's power consumption while still granting the optimum heat transfer performance. Different objectives could also be featured in the optimisation phase, such as material minimisation, volume reduction, and different definitions of heat transfer effectiveness, here taken into account through the introduction of the HTR. This parameter is based on the HTF flow heat capacity, the heat transfer effectiveness, and the maximum heat rate required by the LOHC dehydrogenation reaction.

HTR only needs to reach a certain threshold value and is not to be maximised since no significant kinetic improvements would be achieved once the threshold value is reached. Although HTR values higher than the threshold do not significantly improve the thermodynamic performance, the associated working conditions would most likely require a higher HTF velocity with a marked increase in power consumption.

The significant number of different parameter combinations that satisfy the effectiveness lower bound with similar energy requirements hints at relatively flexible conditions, and additional constraints could likely be included without hindering the system's performance.

This design strategy could be applied to other reactor types (such as PFRs), although the lumped-parameter hypothesis would need to be tested again. Fast and simple implementation of dedicated components in object-based programming languages will then be possible, allowing for a straightforward analysis of complex energy systems, including dynamic simulation and control strategies.

CRediT authorship contribution statement

Marco Gambini: Validation, Visualisation. **Federica Guarnaccia:** Conceptualisation, Methodology, Software, Validation, Writing - Original Draft, Writing - Review & Editing, Visualisation. **Michele Manno:** Conceptualisation, Methodology,

Validation, Writing - Original Draft, Writing - Review & Editing, Visualisation, Supervision. **Michela Vellini:** Validation, Visualisation.

Declaration of competing interest

The authors declare that they have no known competing financial interests or personal relationships that could have appeared to influence the work reported in this paper.

Nomenclature

A	area (m^2)
b	pressure coefficient (bar^{-1})
c	specific heat (J/(kg K))
C	heat capacity (J/(kg K))
d	tube diameter in coiled reactors (m)
D	diameter (m)
ΔH_r	reaction enthalpy change (J/kg)
E_a	activation energy (J/(mol K))
f	friction factor (–)
g	acceleration of gravity (9.81 m^2/s)
h	convective heat transfer coefficient (W/(m^2 K))
H	reactor height (m)
k_0	pre-exponential factor (l/s)
K	empirical parameter
m	mass (kg)
$\dot{m}$	mass flow rate (kg/s)
n	reaction order (–), impeller rotational speed (s^{-1})
N_p	number of pipes (coiled reactor)
p	pressure (Pa)
P	power (W)
$\dot{Q}$	heat rate (W)
r	reaction rate (mol/s)
R	universal gas constant (8.3145 J/(mol K))
s	pitch between pipes in coiled reactor (m)
S	empirical parameter
t	time (s), thickness (m)
T	temperature (K)
u	specific internal energy (J/kg)
U	overall heat transfer coefficient (W/(m^2 K))
v	velocity (m/s)
V	LOHC volume (m^3)
$\mathbf{x}$	decision variables
w	gravimetric storage capacity (–)

Greek letters

β	angular opening of pipes in coiled reactors (∘)
ϵ	heat exchanger effectiveness (–)
ϵ_f	coils fin efficiency
λ	conductivity (W/(m K))
μ	dynamic viscosity (Pa s)
ρ	density (kg/m^3)

Subscripts

c	coil
cr	critical
C	concentrated (pressure losses)
D	distributed (pressure losses)
e	external (outer)
f	heat transfer fluid
HX	heat transfer between HTF and reactor
i	internal (inner)
imp	impeller
j	jacket
l	liquid organic hydrogen carrier
m	wall material
p	constant pressure
v	constant volume
w	reactor wall

Acronyms

AR	Aspect Ratio
DBT	DiBenzylToluene
DoH	Degree of Hydrogenation
HHV	Higher Heating Value
HTF	Heat Transfer Fluid
HTR	Heat Transfer Ratio
LOHC	Liquid Organic Hydrogen Carrier
MH	Metal Hydride
NEC	N-EthylCarbazole
NTU	Number of Transfer Units
PFR	Plug-Flow Reactor

REFERENCES

[1] Ministerial Council on Renewable Energy. Hydrogen and related issues. Basic hydrogen strategy. dec 2017. https://policy.asiapacificenergy.org/sites/default/files/Basic%20Hydrogen%20Strategy%20%28EN%29.pdf. [Accessed 25 October 2022].

[2] Chu Y. China's new energy vehicle industrial development plan for 2021 to 2035. International Council on Clean Transportation; 2021. https://theicct.org/publication/chinas-new-energy-vehicle-industrial-development-plan-for-2021-to-2035/. [Accessed 25 October 2022].

[3] UK hydrogen strategy. https://assets.publishing.service.gov.uk/government/uploads/system/uploads/attachment_data/file/1011283/UK-Hydrogen-Strategy_web.pdf. [Accessed 25 October 2022].

[4] US Department of Energy. Hydrogen program plan. nov 2020. https://www.hydrogen.energy.gov/pdfs/hydrogen-program-plan-2020.pdf. [Accessed 25 October 2022].

[5] European Commission. The European green deal, 640. FIN; 2019. p. 2019. https://eur-lex.europa.eu/legal-content/EN/ALL/?uri=COM. [Accessed 25 October 2022].

[6] European Commission. REPowerEU: affordable, secure and sustainable energy for Europe. 2022. https://ec.europa.eu/info/strategy/priorities-2019-2024/european-green-deal/repowereu-affordable-secure-and-sustainable-energy-europe_en#repowereu-actions. [Accessed 25 October 2022].

[7] Hassan Q, Abdulateef AM, Hafedh SA, Al-samari A, Abdulateef J, Sameen AZ, et al. Renewable energy-to-green hydrogen: a review of main resources routes, processes and evaluation. Int J Hydrogen Energy 2023;48(46):17383–408. https://doi.org/10.1016/j.ijhydene.2023.01.175.

[8] Bellocchi S, De Falco M, Facchino M, Manno M. Hydrogen blending in Italian natural gas grid: scenario analysis and LCA. J Clean Prod 2023;416:137809. https://doi.org/10.1016/j.jclepro.2023.137809.

[9] Ramsebner J, Haas R, Ajanovic A, Wietschel M. The sector coupling concept: a critical review. WIREs Energy and

Environment 2021;10(4):e396. https://doi.org/10.1002/wene.396.
[10] Lagioia G, Spinelli MP, Amicarelli V. Blue and green hydrogen energy to meet European Union decarbonisation objectives. An overview of perspectives and the current state of affairs. Int J Hydrogen Energy 2023;48(4):1304–22. https://doi.org/10.1016/j.ijhydene.2022.10.044.
[11] Bellocchi S, Colbertaldo P, Manno M, Nastasi B. Assessing the effectiveness of hydrogen pathways: a techno-economic optimisation within an integrated energy system. Energy 2023;263:126017. https://doi.org/10.1016/j.energy.2022.126017.
[12] Bhagavathy S, Thakur J. Green hydrogen: challenges for commercialization. In: IEEE smart grid bulletin; 2022. https://smartgrid.ieee.org/bulletins/february-2021/green-hydrogen-challenges-for-commercialization. [Accessed 25 October 2022].
[13] Hirscher M, Yartys VA, Baricco M, von Colbe JB, Blanchard D, Bowman RC, et al. Materials for hydrogen-based energy storage – past, recent progress and future outlook. J Alloys Compd 2020;827:153548. https://doi.org/10.1016/j.jallcom.2019.153548.
[14] US Department of Energy. Energy requirements for hydrogen gas compression and liquefaction as related to vehicle storage needs. DOE Hydrogen and Fuel Cells Program Record; oct 2009. https://www.hydrogen.energy.gov/pdfs/9013_energy_requirements_for_hydrogen_gas_compression.pdf. [Accessed 25 October 2022].
[15] Al Ghafri SZ, Munro S, Cardella U, Funke T, Notardonato W, Trusler JPM, et al. Hydrogen liquefaction: a review of the fundamental physics, engineering practice and future opportunities. Energy Environ Sci 2022;15:2690–731. https://doi.org/10.1039/D2EE00099G.
[16] Papadias DD, Ahluwalia RK. Bulk storage of hydrogen. Int J Hydrogen Energy 2021;46(70):34527–41. https://doi.org/10.1016/j.ijhydene.2021.08.028.
[17] Moradi R, Groth KM. Hydrogen storage and delivery: review of the state of the art technologies and risk and reliability analysis. Int J Hydrogen Energy 2019;44(23):12254–69. https://doi.org/10.1016/j.ijhydene.2019.03.041.
[18] Andersson J, Grönkvist S. Large-scale storage of hydrogen. Int J Hydrogen Energy 2019;44(23):11901–19. https://doi.org/10.1016/j.ijhydene.2019.03.063.
[19] Aakko-Saksa PT, Cook C, Kiviaho J, Repo T. Liquid organic hydrogen carriers for transportation and storing of renewable energy – review and discussion. J Power Sources 2018;396:803–23. https://doi.org/10.1016/j.jpowsour.2018.04.011.
[20] Rong Y, Chen S, Li C, Chen X, Xie L, Chen J, et al. Techno-economic analysis of hydrogen storage and transportation from hydrogen plant to terminal refueling station. Int J Hydrogen Energy 2023. https://doi.org/10.1016/j.ijhydene.2023.01.187.
[21] Correa G, Volpe F, Marocco P, Muñoz P, Falagüerra T, Santarelli M. Evaluation of levelized cost of hydrogen produced by wind electrolysis: Argentine and Italian production scenarios. J Energy Storage 2022;52:105014. https://doi.org/10.1016/j.est.2022.105014.
[22] Muthukumar P, Kumar A, Afzal M, Bhogilla S, Sharma P, Parida A, et al. Review on large-scale hydrogen storage systems for better sustainability. Int J Hydrogen Energy 2023. https://doi.org/10.1016/j.ijhydene.2023.04.304.
[23] Taube M, Rippin DWT, Cresswell DL, Knecht W. A system of hydrogen-powered vehicles with liquid organic hydrides. Int J Hydrogen Energy 1983;8(3):213–25. https://doi.org/10.1016/0360-3199(83)90067-8.
[24] Bourane A, Elanany M, Pham TV, Katikaneni SP. An overview of organic liquid phase hydrogen carriers. Int J Hydrogen Energy 2016;41(48):23075–91. https://doi.org/10.1016/j.ijhydene.2016.07.167.
[25] Brückner N, Obesser K, Bösmann A, Teichmann D, Arlt W, Dungs J, et al. Evaluation of industrially applied heat-transfer fluids as liquid organic hydrogen carrier systems. ChemSusChem 2014;7(1):229–35. https://doi.org/10.1002/cssc.201300426.
[26] Pez G, Scott A, Cooper A, Cheng H. Hydrogen storage by reversible hydrogenation of pi-conjugated substrates. URL US Patent 2008;7. https://www.osti.gov/biblio/1531566. 429,372.
[27] Niermann M, Beckendorff A, Kaltschmitt M, Bonhoff K. Liquid organic hydrogen carrier (LOHC) – assessment based on chemical and economic properties. Int J Hydrogen Energy 2019;44(13):6631–54. https://doi.org/10.1016/j.ijhydene.2019.01.199.
[28] Díaz E, Rapado-Gallego P, Ordóñez S. Systematic evaluation of physicochemical properties for the selection of alternative liquid organic hydrogen carriers. J Energy Storage 2023;59:106511. https://doi.org/10.1016/j.est.2022.106511.
[29] Cho JY, Kim H, Oh JE, Park BY. Recent advances in homogeneous/heterogeneous catalytic hydrogenation and dehydrogenation for potential liquid organic hydrogen carrier (LOHC) systems. Catalysts 2021;11(12):1497. https://doi.org/10.3390/catal11121497.
[30] EU Commission. Efficient system for dehydrogenation of liquid organic hydrogen carriers for application to long distance transportations. Topic ID: HORIZON-JTI-CLEANH2-2022-02-05 Funding & tender opportunities 2022. https://bit.ly/3N1cO6t. [Accessed 25 October 2022].
[31] Dong Y, Yang M, Mei P, Li C, Li L. Dehydrogenation kinetics study of perhydro-N-ethylcarbazole over a supported Pd catalyst for hydrogen storage application. Int J Hydrogen Energy 2016;41(20):8498–505. https://doi.org/10.1016/j.ijhydene.2016.03.157.
[32] Kiermaier S, Lehmann D, Bösmann A, Wasserscheid P. Dehydrogenation of perhydro-N-ethylcarbazole under reduced total pressure. Int J Hydrogen Energy 2021;46(29):15660–70. https://doi.org/10.1016/j.ijhydene.2021.02.128.
[33] Dennis J, Bexten T, Petersen N, Wirsum M, Preuster P. Model-based analysis of a liquid organic hydrogen carrier (LOHC) system for the operation of a hydrogen-fired gas turbine. J Eng Gas Turbines Power 2021;143:031011. https://doi.org/10.1115/1.4048596. 02.
[34] Peters R, Deja R, Fang Q, Nguyen VN, Preuster P, Blum L, et al. A solid oxide fuel cell operating on liquid organic hydrogen carrier-based hydrogen – a kinetic model of the hydrogen release unit and system performance. Int J Hydrogen Energy 2019;44(26):13794–806. https://doi.org/10.1016/j.ijhydene.2019.03.220.
[35] Yang Y, Yao J, Wang H, Yang F, Wu Z, Zhang Z. Study on high hydrogen yield for large-scale hydrogen fuel storage and transportation based on liquid organic hydrogen carrier reactor. Fuel 2022;321:124095. https://doi.org/10.1016/j.fuel.2022.124095.
[36] Gambini M, Guarnaccia F, Di Vona ML, Manno M, Vellini M. Liquid organic hydrogen carriers: development of a thermodynamic and kinetic model for the assessment of hydrogenation and dehydrogenation processes. Int J Hydrogen Energy 2022;47(65):28034–45. https://doi.org/10.1016/j.ijhydene.2022.06.120.
[37] Garvin J. Understand the thermal design of jacketed vessels. Chem Eng Prog 1999;95(6):61–8.
[38] Lienhard IVJH, Lienhard VJH. A heat transfer textbook. 5th ed. Cambridge, MA: Phlogiston Press; 2020 URL http://ahtt.mit.edu.Version.5.10.

[39] Kowalski L, Duszczyk J, Katgerman L. Thermal conductivity of metal powder-polymer feedstock for powder injection moulding. J Mater Sci 1999;34(1–5). https://doi.org/10.1023/A:1004424401427.
[40] Jones J, Poulikakos D, Orozco J. Mixed convection from a rotating horizontal heated cylinder placed in a low-speed wind tunnel. Int J Heat Fluid Flow 1988;9:165–73. https://doi.org/10.1016/0142-727X(88)90067-7.
[41] White FM. Fluid mechanics. McGraw-Hill; 2009. ISBN 978-0-07-352934-9.
[42] Scargiali F, Tamburini A, Caputo G, Micale G. On the assessment of power consumption and critical impeller speed in vortexing unbaffled stirred tanks. Chem Eng Res Des 2017;123:99–110. https://doi.org/10.1016/j.cherd.2017.04.035.
[43] Wan C, An Y, Xu G, Kong W. Study of catalytic hydrogenation of n-ethylcarbazole over ruthenium catalyst. Int J Hydrogen Energy 2012;37(17):13092–6. https://doi.org/10.1016/j.ijhydene.2012.04.123.12th.CHEC.
[44] Bell IH, Wronski J, Quoilin S, Lemort V. Pure and pseudo-pure fluid thermophysical property evaluation and the open-source thermophysical property library CoolProp. Ind Eng Chem Res 2014;53(6):2498–508. https://doi.org/10.1021/ie4033999.
[45] Green DW, Perry RH. Perry's chemical engineers' handbook. McGraw-Hill; 2008. ISBN 978-0071422949.
[46] Gambill WR. How to estimate mixtures viscosities. Chem Eng 1959;66:151–2.
[47] Bell C, Cortes-Pena YR. Chemicals 1.1.2 documentation: thermal conductivity. URL, https://chemicals.readthedocs.io/chemicals.thermal_conductivity.html. [Accessed 18 December 2022].
[48] Gambini M. Metal hydride energy systems performance evaluation. Part A: dynamic analysis model of heat and mass transfer. Int J Hydrogen Energy 1994;19(1):67–80. https://doi.org/10.1016/0360-3199(94)90179-1.
[49] Berger Bioucas FE, Piszko M, Kerscher M, Preuster P, Rausch MH, Koller TM, et al. Thermal conductivity of hydrocarbon liquid organic hydrogen carrier systems: measurement and prediction. J Chem Eng Data 2020;65(10):5003–17. https://doi.org/10.1021/acs.jced.0c00613.
[50] He T, Pei Q, Chen P. Liquid organic hydrogen carriers. J Energy Chem 2015;24(5):587–94. https://doi.org/10.1016/j.jechem.2015.08.007.
[51] Rao N, Lele AK, Patwardhan AW. Optimization of liquid organic hydrogen carrier (LOHC) dehydrogenation system. Int J Hydrogen Energy 2022;47(66):28530–47. https://doi.org/10.1016/j.ijhydene.2022.06.197.
[52] Furukawa H, Kamiya T, Kato Y. Correlation of power consumption of double impeller based on impeller spacing in laminar region. Int J Chem Eng 2019;2019:4564589. https://doi.org/10.1155/2019/4564589.